

Provided for non-commercial research and education use.  
Not for reproduction, distribution or commercial use.

Volume 77, December 2013 ISSN 0010-938X



# CORROSION SCIENCE

The Journal on Environmental Degradation of Materials and its Control  
Editor-in-Chief: G. T. BURSTEIN, University of Cambridge, U.K.  
An Official Journal of the Institute of Corrosion

## CONTENTS

<b>Letter</b>	
K. C. KIM, K. R. LIM, E. S. LEE, W. T. KIM, A. GIBERTI, J. ECKERT and D. H. KIM	1 Thermal stability of amorphous oxide in $Al_{72}Ni_{28}$ metallic glass
<b>Review</b>	
M. MORCHILLO, B. CHICO, I. DIAZ, H. CANO and D. DE LA FUENTE	6 Atmospheric corrosion data of weathering steels. A review
<b>Papers</b>	
X. XIONG, Y.-J. WANG, G.-D. LI, Z.-C. CHEN, W. SUN and Z.-G. WANG	25 HfC/ZrC ablation protective coating for carbon/carbon composites
J. P. KNOWLES, G. RULE and M. BRIBLEY	31 The morphology and anisotropic growth kinetics of cerium hydride reaction sites
K. SAYIN and D. KARAKAS	37 Quantum chemical studies on the some inorganic corrosion inhibitors
J. MÜLLER, B. LAIK and I. GULLOIF	46 $\alpha$ -CuSn bronzes in sulphate medium: Influence of the tin content on corrosion processes
J. M. CALDERON MORENO, E. VASILESCU, P. DROB, P. OUSCANSU, C. VASILESCU, S. I. DROB and M. POPA	52 Surface and electrochemical characterization of a new ternary titanium based alloy behaviour in electrolytes of varying pH
E. PANABIERE, N. EMERY, S. BACH, J.-P. PEREIRA RAMOS and P. WILLMANN	64 Investigation of the chemical stability of $Li-MnN_4$ in air
R. WÜNSINGER, I. MARTINA, CH. KLEBER and M. SCHREINER	69 Influence of relative humidity and ozone on atmospheric silver corrosion
H. SUN, L. LIU, Y. LI, L. MA and Y. YAN	77 The performance of Al-Zn-In-Mg-Ti sacrificial anode in simulated deep water environment
W. W. FOCKE, N. S. NHALAPO and E. VUORINEN	88 Thermal analysis and FTIR studies of volatile corrosion inhibitor model systems
P. FUNTILAKIDIS, Y. LI, N. TANG and A. CHESA	97 Enhancement of corrosion resistance of Fe-Cr-Mo alloy to molten Al by thermal oxidation in air

*Contents continued on outside back cover*

<http://www.elsevier.com/locate/corsci>

This article appeared in a journal published by Elsevier. The attached copy is furnished to the author for internal non-commercial research and education use, including for instruction at the authors institution and sharing with colleagues.

Other uses, including reproduction and distribution, or selling or licensing copies, or posting to personal, institutional or third party websites are prohibited.

In most cases authors are permitted to post their version of the article (e.g. in Word or Tex form) to their personal website or institutional repository. Authors requiring further information regarding Elsevier's archiving and manuscript policies are encouraged to visit:

<http://www.elsevier.com/authorsrights>



Contents lists available at ScienceDirect

## Corrosion Science

journal homepage: [www.elsevier.com/locate/corsci](http://www.elsevier.com/locate/corsci)

# The effect of aerobic corrosion on anaerobically-formed sulfide layers on carbon steel in dilute near-neutral pH saline solutions

B.W.A. Sherar<sup>a,\*</sup>, P.G. Keech<sup>b</sup>, D.W. Shoesmith<sup>c</sup><sup>a</sup> Blade Energy Partners, Ltd., 16285 Park 10 Place, Suite 600, Houston, TX 77084, United States<sup>b</sup> Nuclear Waste Management Organization, 22 St. Clair Avenue East, Toronto, ON M4T 2S3, Canada<sup>c</sup> University of Western Ontario, Department of Chemistry, 1151 Richmond Street, London, ON N6A 5B7, Canada

## ARTICLE INFO

## Article history:

Received 3 July 2013

Accepted 17 August 2013

Available online 28 August 2013

## Keywords:

A. Carbon steel

B. Polarization

B. SEM

B. Raman spectroscopy

C. Oxygen reduction

C. Microbiological corrosion

## ABSTRACT

The aerobic corrosion of pipeline steel was investigated in an aqueous sulfide solution by monitoring the corrosion potential and periodically measuring the polarization resistance. The properties and composition of the corrosion product deposits formed were determined using scanning electron microscopy, energy dispersive X-ray analysis, and Raman spectroscopy. The establishment of aerobic conditions leads to corrosion and (oxyhydr)oxide deposition beneath the anaerobically-formed mackinawite film originally present on the steel surface. This leads to blistering and spalling of the sulfide film. Chemical conversion of the mackinawite to Fe(III) (oxyhydr)oxides also occurs but is a relatively slow reaction.

© 2013 Elsevier Ltd. All rights reserved.

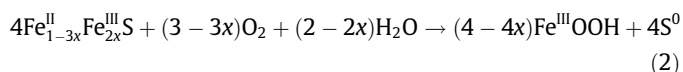
## 1. Introduction

An integrity system based on coatings and cathodic protection (CP) protects buried gas transmission pipelines. If coatings disbond, exposing the steel to groundwater, the effectiveness of the CP system becomes inhibited and the underlying steel becomes susceptible to corrosion [1,2]. Based primarily on field inspections of coating failure sites, TransCanada PipeLines Ltd. (TCPL, Calgary, Alberta, Canada) has proposed six corrosion scenarios that lead to pipeline damage [1,2]. One particularly damaging scenario involves anaerobic corrosion with microbial effects which subsequently turn aerobic, and accounts for 17% of all reported coating failures [1,2]. Reported corrosion rates for this scenario can be as high as 2–5 mm yr<sup>-1</sup> [1,2]. While anaerobic microbial activity may decrease as conditions become more oxidizing, the anaerobically-formed Fe(II) sulfides can oxidize to Fe(III)-containing oxides and elemental sulfur, a process that leads to further pipeline damage, including localized corrosion [2,3].

Recent studies have addressed the Fe/S/H<sub>2</sub>O/O<sub>2</sub> system [4–7]. Bourdoiseau et al. [4] monitored the oxidation of Fe(II)-mackinawite (Fe<sub>1+x</sub>S) under wet oxidizing conditions. The first oxidation stage leads to the formation of an Fe(III)-containing mackinawite;



As oxidation proceeds, transformation to Fe(III) oxy/hydroxides and elemental sulfur occurs



Unreacted Fe(III)-containing mackinawite can also react to form greigite (Fe<sup>II</sup>Fe<sup>III</sup>S<sub>4</sub>) [7], which may further convert to form Fe(III) (oxyhydr)oxides and pyrite, FeS<sub>2</sub>, in air [4],



These studies indicate that films formed microbiologically on pipelines will be reactive under dry out conditions when air becomes available. These anaerobic to aerobic transformations may be very important in determining the high corrosion rates observed following a transition from microbiologically induced corrosion (MIC) under anaerobic conditions to aerobic conditions.

In an attempt to develop corrosion mechanisms that reflect external pipeline conditions, we have previously investigated the effect of inorganic sulfide on carbon steel corrosion in solutions containing chloride, bicarbonate, and sulfate (pH 8.9) under both anaerobic [8] and aerobic [6] conditions. The experiments generated three distinct observations:

- (1) On a steel surface covered with anaerobically-formed magnetite (Fe<sub>3</sub>O<sub>4</sub>)/siderite (FeCO<sub>3</sub>), sulfide causes an increase in corrosion rate initially within pores in the film. Sulfide

\* Corresponding author. Tel.: +1 281 961 1283; fax: +1 281 206 2005.

E-mail address: [bsherar@blade-energy.com](mailto:bsherar@blade-energy.com) (B.W.A. Sherar).

**Table 1**  
Expected Raman peak positions for various iron phases.

Compound	Composition	Raman shift ( $\text{cm}^{-1}$ )	References
Chukanovite	$\text{Fe}(\text{OH})_2\text{CO}_3$	690, 715, 760, 780, 840, 955, 1066	[19]
Hematite	$\alpha\text{-Fe}_2\text{O}_3$	226, 292, 406, 495, 600, 700, 226, 245, 292, 412, 499, 610, 1318	[15] [18]
Goethite	$\alpha\text{-FeOOH}$	297, 392, 484, 564, 674	[15]
Mackinawite	$\text{Fe}_{(1+x)}\text{S}$	254, 307, 318, 354	[5]
Maghemite	$\gamma\text{-Fe}_2\text{O}_3$	358, 499, 678, 710	[15]
Magnetite	$\text{Fe}_3\text{O}_4$	297, 523, 666	[15]
Siderite	$\text{FeCO}_3$	734, 1089, 1443, 1736	[16]
Sulfur	$\text{S}_8$	150, 220, 475	[17]

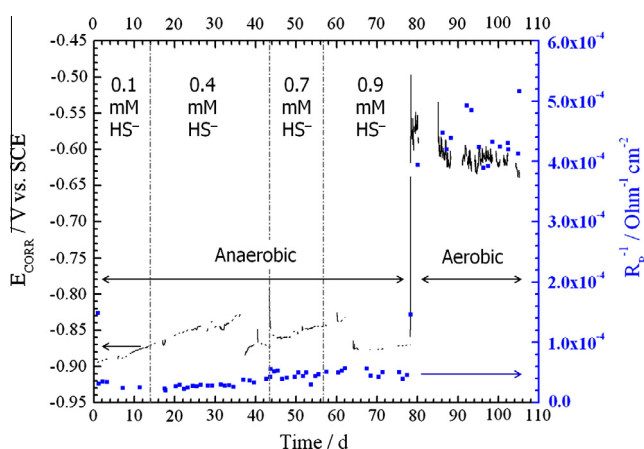


**Fig. 1.** Corrosion potential ( $E_{\text{CORR}}$ ) and inverse polarization resistances ( $R_p^{-1}$ , data points) measured on steel under anaerobic (up to 78 days) and aerobic conditions. Aliquots of  $\text{HS}^-$  were added at the times indicated by the vertical lines, and the labeled  $\text{HS}^-$  concentrations are cumulative for that specific period.

initiates a conversion from magnetite to mackinawite but the sulfide deposit formed does not passivate the surface and leads to a steady on-going increase in corrosion rate [8].

- (2) When sulfide is present from the beginning of steel exposure to an anaerobic dilute simulated groundwater, a “passive” layer of mackinawite is formed. The corrosion rate is independent of  $[\text{HS}^-]$ , indicating that it is controlled by the properties of the sulfide film [8].
- (3) If the steel surface is covered by aerobically-formed goethite-covered tubercles, sulfide addition causes surges in corrosion rate, followed by an apparent partial suppression of corrosion; although  $R_p^{-1}$  and  $E_{\text{CORR}}$  values indicate the corrosion rate is higher than those measured during the aerobic corrosion (without sulfide) period. On-going exposure to aqueous sulfide leads to a slow corrosion process as the goethite-covered surface surrounding the tubercles is converted to mackinawite [6].

In this study we have investigated the influence of aerobic corrosion on an anaerobically-formed mackinawite film using the methodologies previously developed [6,8–12]. Corrosion was monitored over a 106 day period by following the corrosion potential ( $E_{\text{CORR}}$ ) and periodically measuring the polarization resistance ( $R_p$ ) using linear polarization resistance (LPR) measurements. Subsequently, the morphology and composition of the corrosion product deposits were determined using scanning electron microscopy (SEM) and energy dispersive X-ray spectroscopy (EDX), and Raman spectroscopy.

## 2. Experimental details

### 2.1. Materials and electrode preparation

Experiments were performed on X65 carbon steel (0.07 C; 1.36 Mn; 0.013 P; 0.002 S; 0.26 Si; 0.01 Ni; 0.2 Cr; 0.011 Al (wt.%) supplied by TCPL. For corrosion measurements, a cubic coupon,  $1.0 \text{ cm} \times 1.0 \text{ cm} \times 1.0 \text{ cm}$ , was cut from metal plates and fitted with a carbon steel welding rod (4 mm diameter) to facilitate connection to external equipment. The electrode was then encased in a high performance epoxy resin (Ameron pearl grey resin and 90HS cure) so that only a single face was exposed to the solution. Prior to the experiment, the exposed face (surface area  $1.0 \text{ cm}^2$ ) was ground sequentially on 180, 320, 600, and 1200 grit SiC paper, ultrasonically cleaned for 10 min in deaerated, ultrapure de-ionized water (Millipore, conductivity:  $18.2 \text{ M}\Omega \text{ cm}$ ) mixed with methanol (ratio of 1:1) to remove organic contaminants, and finally ultrasonically cleaned in deaerated, Millipore water.

### 2.2. Solution and gas exposure conditions

The experiment was conducted in a dilute simulated groundwater containing  $5.2 \text{ mmol L}^{-1} \text{ NaHCO}_3 + 6.2 \text{ mmol L}^{-1} \text{ Na}_2\text{CO}_3 + 0.6 \text{ mmol L}^{-1} \text{ NaCl} + 0.5 \text{ mmol L}^{-1} \text{ Na}_2\text{SO}_4 + 0.1 \text{ mol L}^{-1} \text{ NaClO}_4$ . All chemicals were research grade. These ion concentrations were comparable to those encountered in natural near surface groundwaters in regions of interest (e.g. Northern Ontario and Alberta, Canada) [13], while the perchlorate was added to increase the conductivity. This anion is not expected to have any significant influence on the corrosion behavior of the steel [14]. The exposure

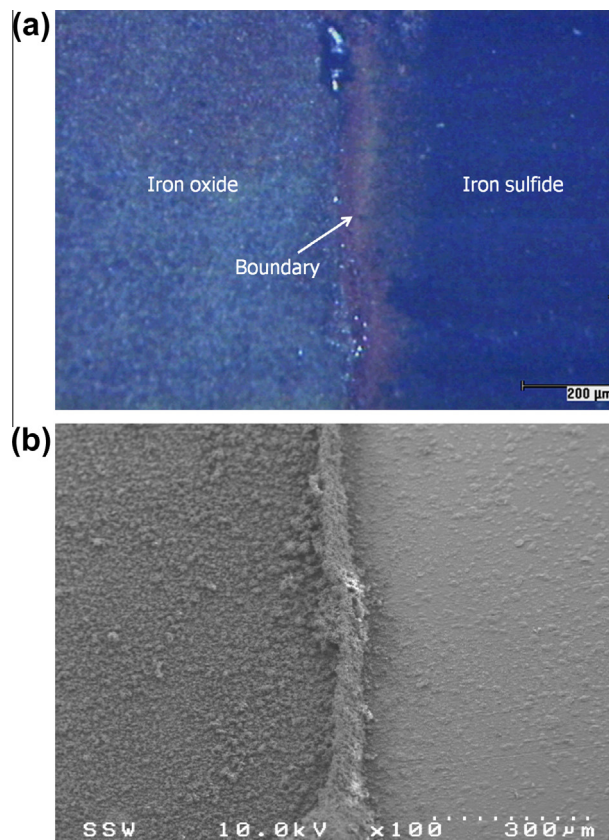


**Fig. 2.** (a) Optical image and (b) SEM micrograph of the steel surface after anaerobic (78 days) followed by aerobic (26 days) corrosion in a sulfide-containing solution. The boundary (corrosion “front”) separates a surface only slightly corroded (iron sulfide) from a surface severely corroded (iron oxide).

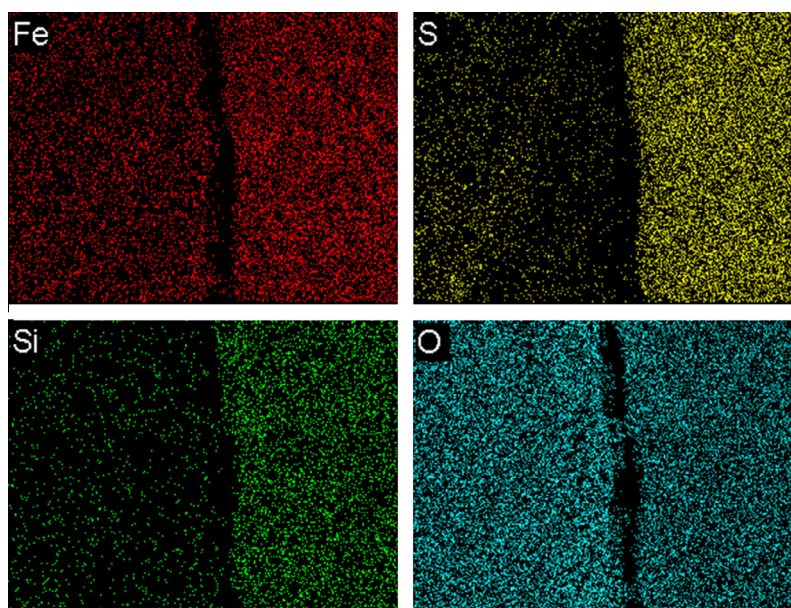


Fig. 3. EDX elemental maps for Fe, S, Si and O recorded on the surface shown Fig. 2.

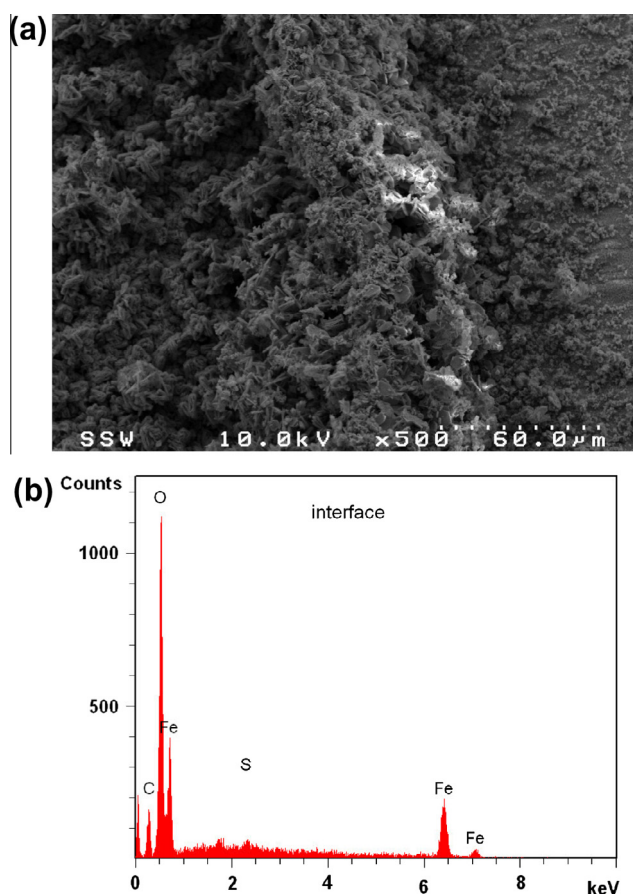


Fig. 4. (a) SEM micrograph of the corrosion front shown in Fig. 2; and (b) EDX spot analysis of the same region.

solution pH was set to  $8.90 \pm 0.05$  with NaOH prior to beginning the experiment.

Throughout the anaerobic corrosion period, sequential aliquots of  $\text{HS}^-$  were added (from a  $0.1 \text{ mol L}^{-1} \text{ Na}_2\text{S}\cdot 9\text{H}_2\text{O}$  stock solution) using a micropipette, up to a total concentration of  $0.9 \text{ mmol L}^{-1}$ .

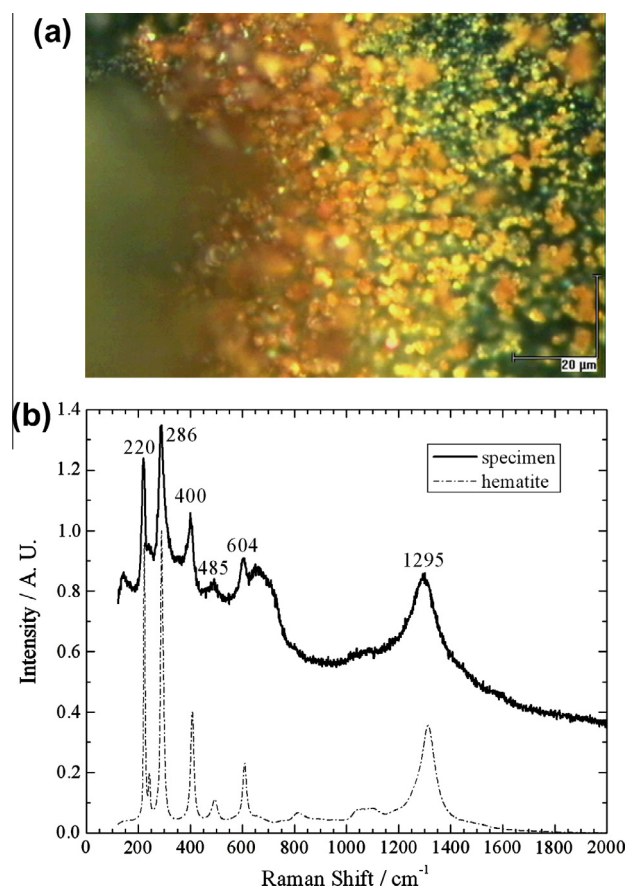


Fig. 5. (a) Optical image and (b) Raman spectrum of the corrosion front shown in Fig. 2. Also, shown in (b) is a reference spectrum for hematite.

Aliquots of  $\text{HS}^-$  were added at various stages, and the labeled  $\text{HS}^-$  concentration is that prevailing during a specific period.

Anaerobic conditions were maintained by placing the cell in an anaerobic chamber ( $[\text{O}_2] < 1 \text{ ppm}$ ), while aerobic conditions were maintained by venting the cell with air after removal from the anaerobic chamber.

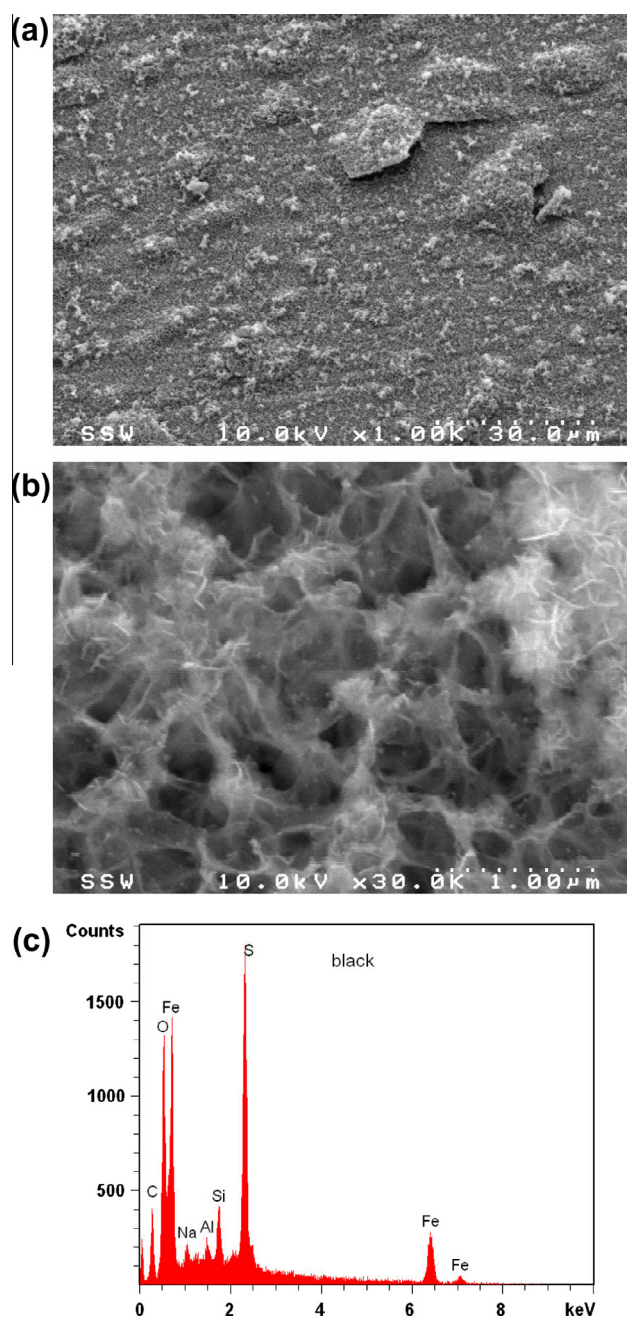


Fig. 6. (a) Low magnification and (b) high magnification SEM micrographs of the sulfide-rich region shown in Fig. 2; (c) EDX spectra recorded on the same location.

### 2.3. Electrochemical cell and equipment

The experiment was conducted in a standard three-compartment, three-electrode glass electrochemical cell. The counter electrode was a Pt foil (99.9% purity, Alfa Aesar) and the reference electrode was a commercial saturated calomel electrode (SCE; 241 mV vs. SHE) (Radiometer Analytical, Loveland, CO.). The cell was either housed in a grounded Faraday cage or placed in a grounded anaerobic chamber; both locations minimize external noise. Prior to immersion of the steel coupon, the electrolyte solution was purged for at least 1 h using ultra high purity Ar (Praxair, Mississauga, ON) to generate anaerobic conditions. A Solartron 1287 Potentiostat, running Corrware software (version 2.6 Scribner Associates) was used to control applied potentials and to record current responses.

### 2.4. Experimental procedure

Prior to the experiment, the electrode was cathodically cleaned at  $-1.3 V_{SCE}$  for 1 min to minimize any air-formed surface oxide. The potential was then stepped to  $-1.1 V_{SCE}$  for 1 min to prevent  $H_2$  production and clear the surface of  $H_2$  bubbles while maintaining cathodic protection. Subsequently, the corrosion potential ( $E_{CORR}$ ) was monitored continuously, except for brief periods (every 24 h) during which  $R_p$  was measured using the linear polarization resistance (LPR) technique. LPR measurements were performed by scanning the potential  $\pm 10$  mV (root mean square) from  $E_{CORR}$  at a scan rate of  $0.1 mV s^{-1}$ ; a single measurement required a total of 10 min. The current values observed during LPR measurements ranged from 5 to  $50 \mu A cm^{-2}$  under anaerobic conditions, and from 100 to  $150 \mu A cm^{-2}$  under aerobic conditions. At the conclusion of the experiment, the electrode was removed for surface analysis.

### 2.5. Surface analysis

Upon removal from the cell the electrode was quickly rinsed in deaerated, Millipore water to prevent the precipitation of the electrolyte during drying in an anaerobic chamber. After its removal from the anaerobic chamber, the electrode was analyzed by SEM/EDX and optical microscopy/Raman spectroscopy as quickly as possible, to minimize air-induced conversions that may occur to corrosion products. SEM/EDX analyses were performed on a Hitachi S4500 field emission SEM using a primary beam voltage of 10 keV; this instrument was equipped with an X-ray detector for EDX. To identify iron oxide/sulfide phases, a Renishaw 2000 Raman spectrometer, with a 632.8 nm laser line, filtered to 25 and 50% of maximum power at 15 mW (depending upon the specimen) to minimize laser induced oxidation of the surface, and an optical microscope with a  $50\times$  magnification objective lens, were used. The expected Raman peak positions for various Fe oxide/sulfide phases are summarized in Table 1 [5,15–19].

## 3. Results and discussion

Fig. 1 shows the  $E_{CORR}$ , and  $R_p^{-1}$  values (data points) recorded as a function of exposure time. A detailed description of the corrosion behavior and surface analysis under anaerobic conditions (for times <day 78) was described previously [8]. Over this period both  $E_{CORR}$  ( $\sim -900 mV_{SCE}$ ) and the  $R_p^{-1}$  ( $[4.5 \pm 0.6] \times 10^{-5} ohm s^{-1} cm^{-2}$ ) remain fairly constant, despite the incremental increase in sulfide concentration up to  $0.9 mmol L^{-1}$  [8]; the incremental increases are indicated in Fig. 1. The corrosion rate (which is proportional to  $R_p^{-1}$ ) is independent of  $[HS^-]$ , indicating that the rate is limited by the mass transfer related properties of the sulfide film in dilute simulated groundwaters [8]. This trend is consistent with the observations of Newman et al. [20], who found sulfide films to be passivating in the absence of any pre-corrosion of steel substrates. Interestingly, the low  $R_p^{-1}$  in the presence of sulfide, was approximately equal to the value recorded in anaerobic solutions without sulfide ( $[4.4 \pm 1.2] \times 10^{-5} ohm s^{-1} cm^{-2}$ ) [9].

On switching from anaerobic to aerobic conditions on day 78 (Fig. 1),  $E_{CORR}$  increased within a matter of hours to  $-600 mV_{SCE}$ , eventually exceeding  $-500 mV_{SCE}$  within days. This was accompanied by an increase in  $R_p^{-1}$  of approximately one order of magnitude from  $5 \times 10^{-5} ohm s^{-1} cm^{-2}$  prior to aerobic exposure to  $4 \times 10^{-4} ohm s^{-1} cm^{-2}$  immediately after its addition. This immediate response of  $E_{CORR}$  and  $R_p^{-1}$  to the switch to aerobic conditions confirms that the sulfide covered surface is very susceptible to corrosion, and despite some fluctuations, both  $E_{CORR}$  and  $R_p^{-1}$  remain fairly constant over the 26 day aerobic exposure period.

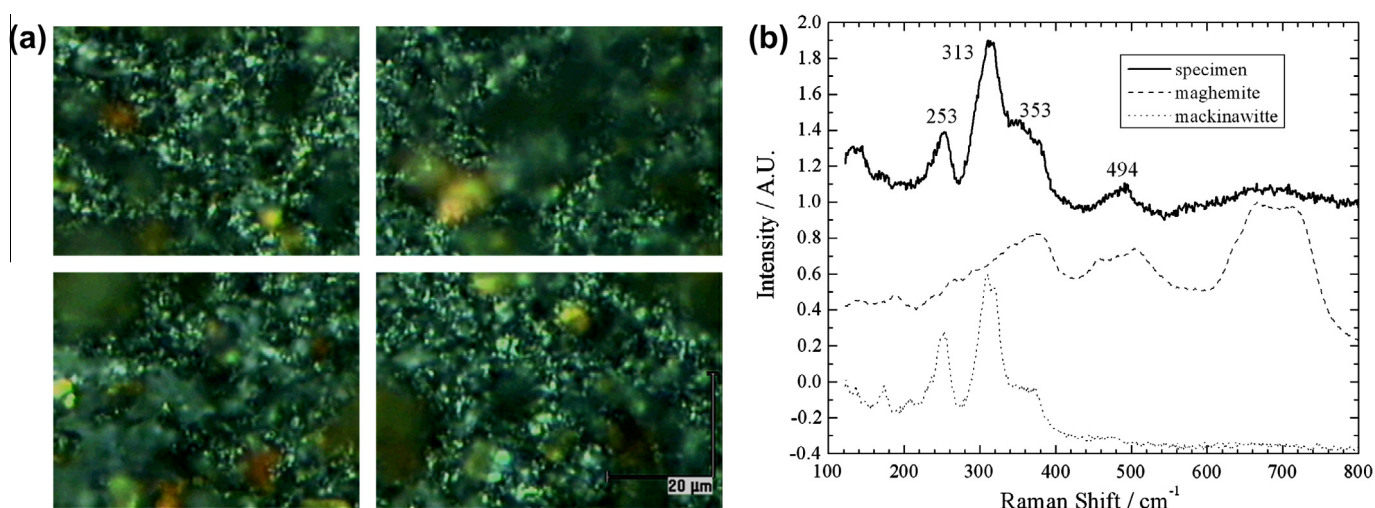


**Fig. 7.** Optical image of a location within the sulfide-rich region (Figs. 2 and 6a and b) and (b) a Raman spectrum recorded at the location of the cross hairs in the image. Also shown in (b) are reference spectra for mackinawite and maghemite.

To support our corrosion experiment and to better understand the stability of, and corrosion processes between, iron oxides and sulfides in general, we have performed a series of surface analyses by SEM/EDX and optical/Raman of the exposed corrosion coupon at various surface features. For a particular location, the corresponding SEM and optical images are both shown throughout as the two imaging techniques are complementary. They provide salient information regarding the microstructure of various surface features (SEM), and the color of the corrosion product deposits (optical) provide additional evidence to support Raman fingerprinting of the various deposits. This methodology is consistent with our previous research on this topic [6,8–12].

Fig. 2a and b shows optical and SEM images of an apparent corrosion “front” on the steel surface, taken on completion of the experiment. To the right of the front (boundary) the SEM image shows a surface only slightly corroded, while to the left a visible deposit has accumulated. The EDX elemental maps in Fig. 3 shows strong signals for O on either side of the boundary, but a markedly stronger S (and Si) signal on the lightly-corroded featureless area to the right. This is consistent with the presence of a dual oxide-sulfide layer in this region. One possible source of silicon was the steel, which is known to contain Si (0.26%). Also, the Fe signal is noticeably stronger in this region, which is consistent with the presence of a thinner corrosion product film. The lack of interpretable EDX signals near the boundary region is presumed to be due to an interference of the topography with X-ray emission during EDX mapping. Thus, to supplement this information, Fig. 4a shows an SEM image and Fig. 4b an EDX spot analysis of the boundary region. The strong O and minor S signals confirm this region is primarily oxide. As shown in the optical image in Fig. 5a, the orange color suggests the deposit is an iron (oxyhydr)oxide; possibly hematite based on the Raman spectrum in Fig. 5b (220, 286, 400, 485, 604, and 1295 cm⁻¹). It is reasonable to presume that this phase may have formed directly during aerobic conditions [15]. Alternatively, the iron phase of the original corrosion front phase may have been maghemite as there is a broad peak between 600 and 700 cm⁻¹ (Fig. 5b). It is also possible that poorly crystallised iron compounds such as ferrihydrite (5Fe<sub>2</sub>O<sub>3</sub>·9H<sub>2</sub>O) and/or feroxyhyte (δ-FeOOH) formed in addition to maghemite, although the in-house reference spectra of maghemite visually matched the best to the corrosion sample. All of these phases are potentially susceptible to heat induced conversion to hematite by the laser; although efforts were made to filter the laser intensity to reduce oxidation of the film.

The SEM micrograph in Fig. 6a shows the film in the S-rich region (i.e., the area on the right of the micrograph in Fig. 2b) is coarse with a light, widely-distributed deposit and a significant number of ruptured or incipient blisters. The magnified image (Fig. 6b) shows a porous structure decorated with a fine fibrous deposit. During previous exposure experiments, the porous structure was present after the initial 78 day anaerobic corrosion period [8]. The fine deposit, however, only appeared after the subsequent 26 day aerobic period within the experiments conducted in this study, suggesting it is a signature of the sulfide to oxide conversion process. The EDX spectrum, Fig. 6c, confirms the presence of both oxide and sulfide in this area; in comparison, oxide was not previously seen [8].

The optical image of this area, Fig. 7a, shows the presence of orange clusters suggesting the partial oxidation of FeS to Fe(III) oxide. Raman spectra recorded in the vicinity of these orange locations are inconclusive, showing no defined peaks that could be matched to known reference spectra. However, the spectrum recorded on the background surface (i.e., at the crosshairs in the optical image, Fig. 7a) clearly shows mackinawite remains the dominant phase with several broad peaks at 253, 313, 353, and 494 cm⁻¹ and the band between 600 and 800 cm⁻¹ suggesting the coexistence of a poorly crystalline (oxyhydr)oxide. Whether or not elemental S is also present, as expected/predicted from reaction 2, cannot be conclusively determined since the Raman peak for S would overlap with the broad peak observed at 494 cm⁻¹.

SEM micrographs of the oxygen-rich region (i.e., the left side of the images in Fig. 2) are shown in Figs. 8a and b. At low magnification, Fig. 8a, the deposits appear as a collection of irregular clusters. At high magnification, however, the individual clusters can be seen to be flower-shaped nanostructures (Fig. 8b). An EDX spot analysis, Fig. 8c, confirms these deposits are primarily oxide as only a minor peak for S is observed. Fig. 9a is an optical image of a number of these flower-shaped deposits. Both Figs. 8a and 9a were both taken on the iron oxide (left side) of Fig. 2a, but do not necessarily overlap as SEM and optical images of the same general area were performed at different times. By morphology alone, it is unclear what iron oxide phase the flower-shaped deposits belong to. Interspersed between the bright crystals, is a finely particulate (oxyhydr)oxide as identified by the dominant, broad Raman peak at 684 cm⁻¹ (Fig. 9b). The deposits appear to be maghemite, although the interpretation is not definitive as the Raman spectra below 600 cm⁻¹ appears smeared; perhaps due to interference from multiple overlapping (oxyhydr)oxide phases. A Raman spectrum of the

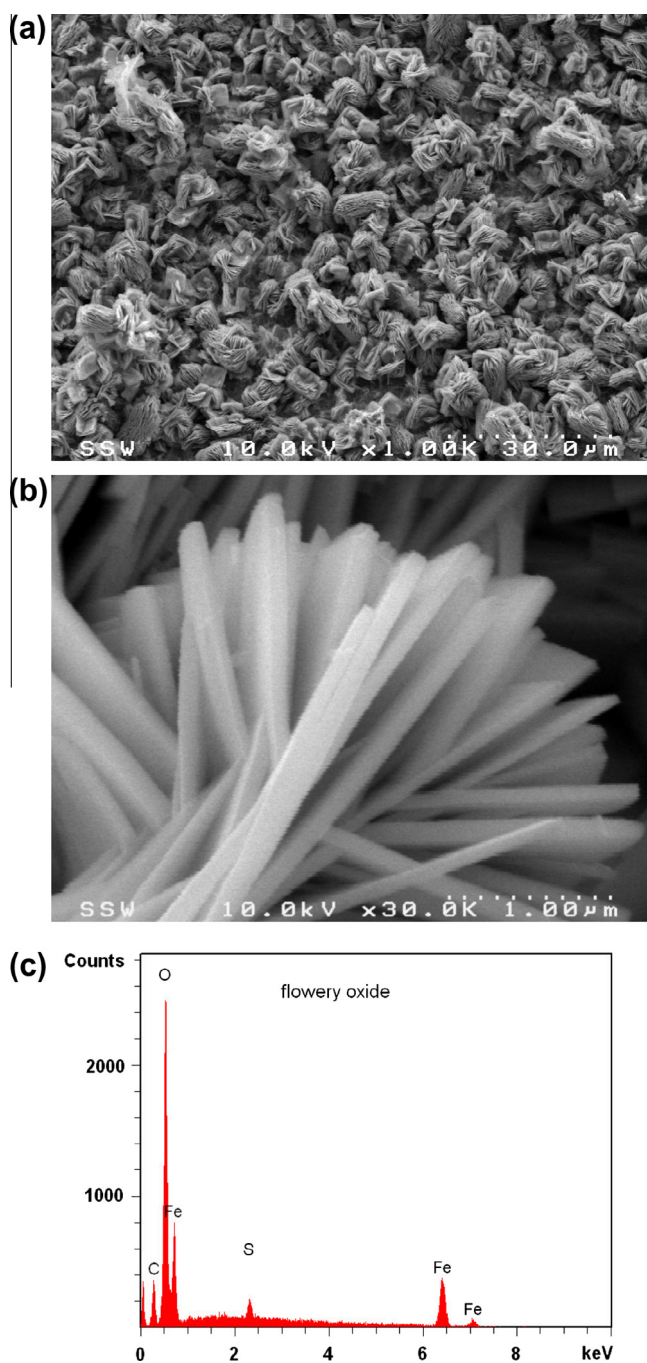


Fig. 8. (a) Low magnification and (b) high magnification SEM micrographs of the oxide-rich region shown in Fig. 2. (c) EDX spot analysis of the same region.

bright crystals shows them to be chukanovite ( $\text{Fe}(\text{OH})_2\text{CO}_3$ , 724 and  $1069\text{ cm}^{-1}$  (Fig. 9c) vs. reference peaks at 715 and  $1070\text{ cm}^{-1}$  [19]). The existence of iron carbonate is likely a remnant of the original anaerobically-formed film; Jack et al. [1] showed that siderite ( $\text{FeCO}_3$ ) and mackinawite coexist under field conditions, and we have previously also observed this compound [8].

In an effort to understand the film conversion processes, we have sought out regions of the surface where different topography exists to try to correlate these features with sulfide/oxide growth periods; Fig. 10 is an example. At the far left of Fig. 10 is the edge of a blister where part of the original sulfide film (formed during the anaerobic period) appears to have detached from the surface. The EDX maps for O and S are also shown. Blisters and areas of de-

tached film were never observed prior to the establishment of aerated conditions [8] and are a feature of the aerobic corrosion process. The absence of an EDX signal for S in this blister region, where the detachment appears to have occurred, implies that the detached layer was the original anaerobically-grown mackinawite layer. The strong signal for S on the scale-covered surface (i.e., the remainder of the surface) indicates the mackinawite layer remained attached elsewhere. (It is possible that the corrosion leading to the oxide formation shown on the left side of the images in Fig. 2 occurred by a similar detachment process.)

Mechanistically, these observations imply corrosion leading to oxide deposition occurred on the steel surface beneath the anaerobically-formed sulfide layer. The alternating rows of high and low S signal may be due to the deposits apparently present on the surface (and visible as small particulates in the SEM image, Fig. 10) in these locations, but may also indicate more extensive undermining of the sulfide film by oxide formation, which enhances its detachment in these areas. The relatively uniform EDX signal for O at all locations in the image (Fig. 10) supports this claim, in that oxide forms regardless of the presence of sulfide.

Collectively, these results indicate that aerobic corrosion can proceed rapidly underneath a weakly adherent mackinawite layer to produce significant quantities of  $\text{Fe}^{\text{III}}$  oxides. For such a process to occur the mackinawite layer must be sufficiently porous to allow oxide formation to initiate on the steel surface but remain chemically stable on the time scale of the experiment; i.e., not rapidly convert to oxides via the mechanism published by Bourdoiseau et al. [4,5]. The proliferation of ruptured and incipient blisters shown in Fig. 10 confirms many sites where corrosion initiates below the previously formed sulfide. That direct conversion of sulfide to oxide is slow at the pH in this experiment is supported by the SEM/EDX analyses in Fig 6, which show only minor amounts of iron oxide on the originally-formed mackinawite. Given the obvious porosity of the mackinawite deposit, many potential locations are available to initiate the aerobic corrosion process below the sulfide layer, which then proceeds rapidly leading to the detachment of the sulfide. Since mackinawite is electrically conducting it is likely that rapid undermining can also be supported by  $\text{O}_2$  reduction on the outside of the film. A corrosion mechanism beneath the iron sulfide, leading to iron sulfide film blistering, would be consistent with the periodic  $E_{\text{CORR}}$  and  $R_p^{-1}$  transients observed in Fig. 1, following the anaerobic to aerobic transition. A schematic illustration of this mechanism is shown in Fig. 11.

The results in this study can be compared to our previous ones [6] in which a period of anaerobic corrosion followed by aerobic corrosion was conducted in the absence of sulfide. In that experiment a similar transition in  $E_{\text{CORR}}$  and rapid increase in  $R_p^{-1}$  was also observed. However, this transition led to the initiation of tubercle-covered pits rather than the undermining process shown to occur in the present case. Subsequently corrosion in the absence of sulfide was concentrated at these tubercle sites, while the remainder of the surface became passive as the magnetite surface layer converted, at least at the oxide/solution interface, to goethite. While the  $R_p^{-1}$  values cannot be directly compared between these experiments since corrosion propagation is very different, this difference in behavior most likely reflects the porosity of the sulfide layer, making it permeable to  $\text{O}_2$ , and its poor adherence to the steel surface.

#### 4. Conclusions

- (1) The influence of switching from anaerobic to aerobic conditions on the corrosion of steel in sulfide solutions has been studied using electrochemical techniques, SEM/EDX, and optical microscopy/Raman spectroscopy.

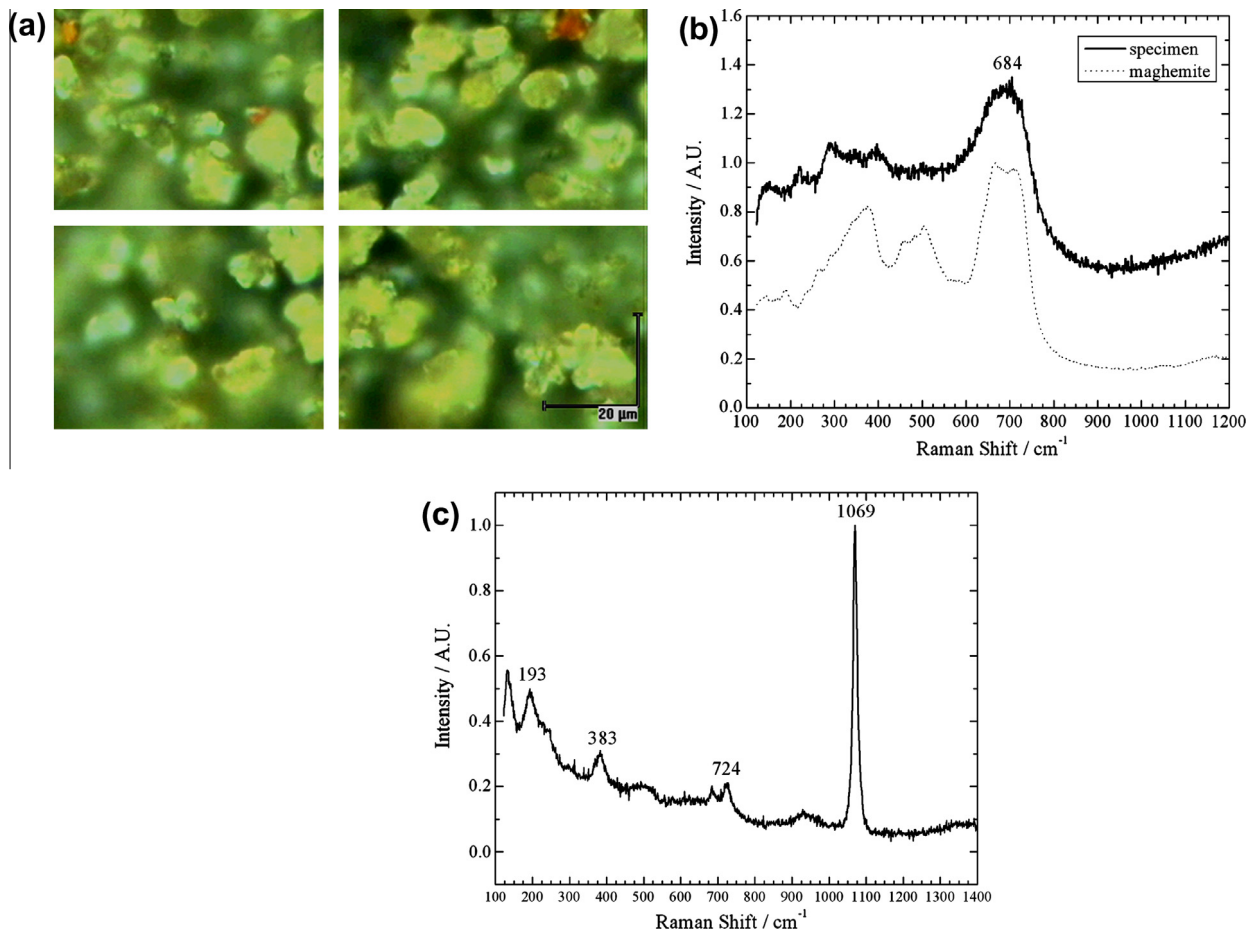


**Fig. 9.** (a) Optical image and Raman spectra of the red deposit (b) and the bright crystals (c) observed within the oxide-rich region shown in Fig. 2 and 8. Also shown in (b) is a reference spectrum for maghemite.

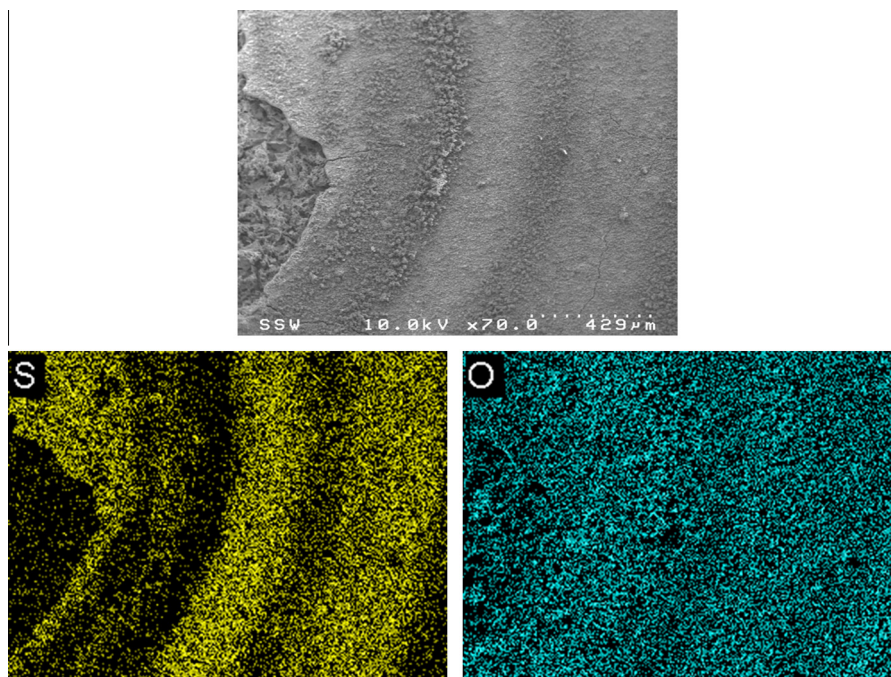


**Fig. 10.** SEM image of a region on the surface of the specimen revealing sulfide blistering (top left) where the mackinawite layer originally present has detached. Also shown are EDX elemental maps of the same area for S and O.

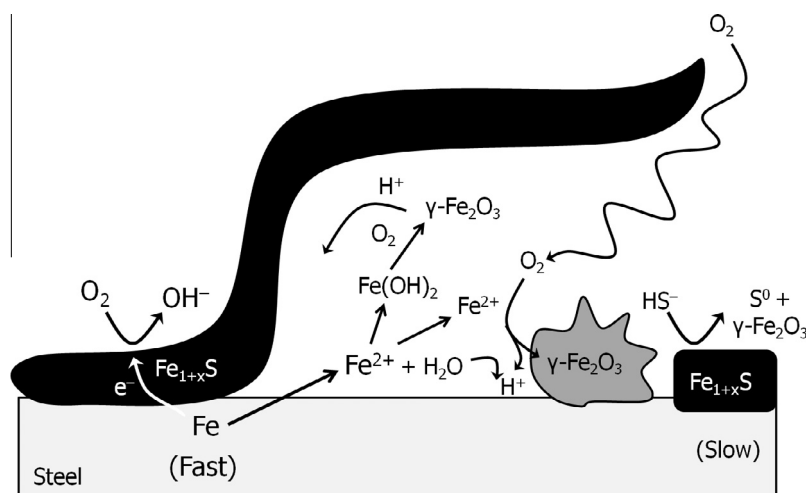


**Fig. 11.** Schematic illustration of the corrosion process occurring on a mackinawite-covered surface under aerobic conditions. Corrosion occurs via a rapid under-deposit process leading to the blistering and spalling of the mackinawite, and by a much slower transformation of the mackinawite layer to any number of (oxyhydr)oxide (e.g., maghemite) and sulfur (slow reaction).

- (2) The anaerobically-formed mackinawite is sufficiently porous to allow direct access of dissolved  $O_2$  to the substrate steel. This leads to a corrosion process beneath the iron sulfide film, yielding maghemite and causes blistering and spalling of the mackinawite layer.
- (3) Chemical conversion of mackinawite to Fe(III) oxide, and possibly  $S^0$ , at the outer sulfide/solution interface also occurs, but is slow by comparison to the corrosion process beneath the sulfide film.

## Acknowledgements

This research was carried out for NOVA Research & Technology Centre (NRTC, Calgary, AB, Canada) and TCPL through an Industrial Postgraduate Scholarship Agreement with the University of Western Ontario and the Canadian Natural Sciences and Engineering Research Council (NSERC, Ottawa, ON). Fraser King, Integrity Corrosion Consulting Ltd., and Robert (Bob) G. Worthingham, Worthingham Professional Services Inc., are gratefully acknowledged by the authors for their guidance and continued support of the research. The reviewer is also acknowledged for providing thoughtful insight into Raman fingerprinting and interpretation.

## References

- [1] T.R. Jack, M.J. Wilmott, R.L. Sutherby, Indicator minerals formed during external corrosion of line pipe, *Materials Performance* 34 (1995) 19–22.
- [2] T.R. Jack, M.J. Wilmott, R.L. Sutherby, R.G. Worthingham, External corrosion of line pipe – A summary of research activities, *Materials Performance* 35 (1996) 18–24.
- [3] E.B. Hansson, M.S. Odziemkowski, R.W. Gillham, Formation of poorly crystalline iron monosulfides: surface redox reactions on high purity iron, spectroelectrochemical studies, *Corrosion Science* 48 (2006) 3767–3783.
- [4] J.A. Bourdoiseau, M. Jeannin, C. Rézazeilles, R. Sabot, P. Refait, The transformation of mackinawite into greigite studied by Raman spectroscopy, *Journal of Raman Spectroscopy* 42 (2011) 496–504.
- [5] J.A. Bourdoiseau, M. Jeannin, R. Sabot, C. Rézazeilles, P. Refait, Characterisation of mackinawite by Raman spectroscopy: effects of crystallisation, drying and oxidation, *Corrosion Science* 50 (2008) 3247–3255.
- [6] B.W.A. Sherar, P.G. Keech, D.W. Shoesmith, The effect of sulfide on the aerobic corrosion of carbon steel in near-neutral pH saline solutions, *Corrosion Science* 66 (2013) 256–262.
- [7] S. Boursiquot, M. Mullet, M. Abdelmoula, J.-M. Genin, J.-J. Ehrhardt, The dry oxidation of tetragonal  $FeS_{1-x}$  mackinawite, *Physics and Chemistry of Minerals* 28 (2001) 600–611.
- [8] B.W.A. Sherar, P.G. Keech, J.J. Noel, R.G. Worthingham, D.W. Shoesmith, The effect of sulfide on carbon steel corrosion behaviour in anaerobic near-neutral pH saline solutions, *Corrosion* 69 (2013) 67–76.
- [9] B.W.A. Sherar, P.G. Keech, Z. Qin, F. King, D.W. Shoesmith, Nominally anaerobic corrosion of carbon steel in near-neutral pH saline environments, *Corrosion* 66 (2010) 045001.
- [10] B.W.A. Sherar, P.G. Keech, D.W. Shoesmith, Carbon steel corrosion under anaerobic-aerobic cycling conditions in near-neutral pH saline solutions. Part 2: Corrosion mechanism, *Corrosion Science* 53 (2011) 3643–3650.
- [11] B.W.A. Sherar, P.G. Keech, D.W. Shoesmith, Carbon steel corrosion under anaerobic-aerobic cycling conditions in near-neutral pH saline solutions – Part 1: Long term corrosion behaviour, *Corrosion Science* 53 (2011) 3636–3642.
- [12] B.W.A. Sherar, I.M. Power, P.G. Keech, S. Mitlin, G. Southam, D.W. Shoesmith, Characterizing the effect of carbon steel exposure in sulfide containing solutions to microbially induced corrosion, *Corrosion Science* 53 (2011) 955–960.
- [13] T.R. Jack, G. Vanboven, M. Wilmott, R.L. Sutherby, R.G. Worthingham, Cathodic protection potential penetration under disbonded pipeline coating, *Materials Performance* 33 (1994) 17–21.
- [14] A.M. Moore, C.H. De Leon, T.M. Young, Rate and extent of aqueous perchlorate removal by iron surfaces, *Environmental Science and Technology* 37 (2003) 3189–3198.
- [15] M.A. Legodi, D. de Waal, The preparation of magnetite, goethite, hematite and maghemite of pigment quality from mill scale iron waste, *Dyes and Pigments* 74 (2007) 161–168.
- [16] R.G. Herman, C.E. Bogdan, A.J. Sommer, D.R. Simpson, Discrimination among carbonate minerals by Raman-spectroscopy using the laser microprobe, *Applied Spectroscopy* 41 (1987) 437–440.
- [17] S.N. White, Laser Raman spectroscopy as a technique for identification of seafloor hydrothermal and cold seep minerals, *Chemical Geology* 259 (2009) 240–252.
- [18] R. Michel, M.R. Ammar, J. Poirier, P. Simon, Phase transformation characterization of olivine subjected to high temperature in air, *Ceramics International* 39 (2013) 5287–5294.
- [19] C. Rézazeilles, P. Refait, Fe(II) hydroxycarbonate  $Fe_2(OH)_2CO_3$  (chukanovite) as iron corrosion product: synthesis and study by fourier transform infrared spectroscopy, *Polyhedron* 28 (2009) 749–756.
- [20] R.C. Newman, K. Rumash, B.J. Webster, The effect of precorrosion on the corrosion rate of steel in neutral solutions containing sulfide – relevance to microbially influenced corrosion, *Corrosion Science* 33 (1992) 1877–1884.